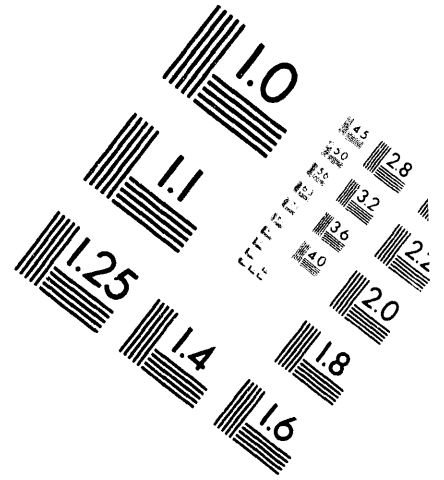
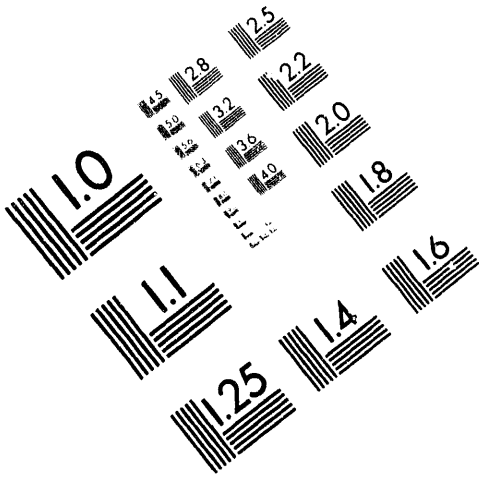




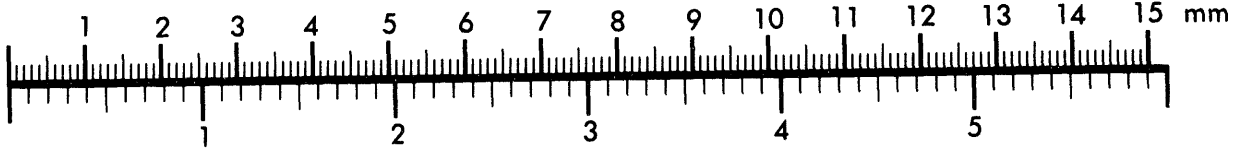
AIM

Association for Information and Image Management

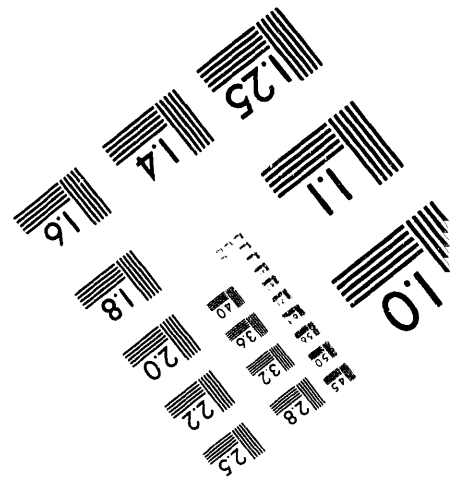
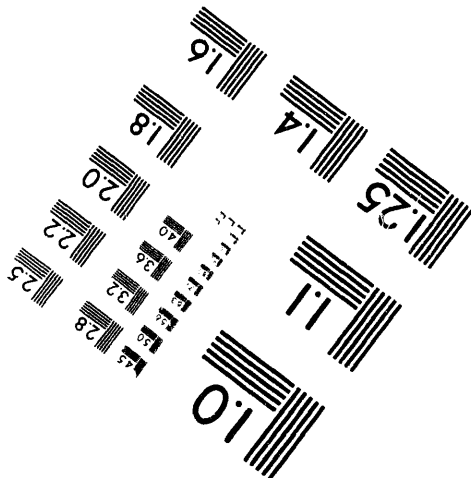
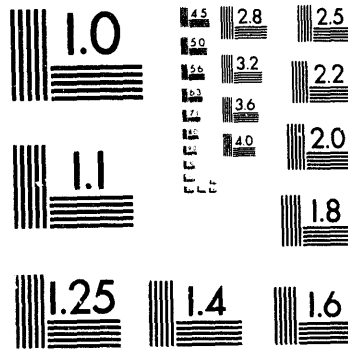
1100 Wayne Avenue, Suite 1100
Silver Spring, Maryland 20910
301/587-8202



Centimeter



Inches



MANUFACTURED TO AIM STANDARDS
BY APPLIED IMAGE, INC.

1 of 1

ANL/TD/CP--83938
CONF-940664--27

**PRESENT UNDERSTANDING OF MHD AND HEAT TRANSFER
PHENOMENA FOR LIQUID METAL BLANKETS**

Igor R. Kirillov
D. V. Efremov Scientific Research
Institute of Electrophysical
Apparatus, 189631 St. Petersburg,
Russia

Claude B. Reed
Fusion Power Program
Technology Development Division
Argonne National Laboratory
Argonne, IL 60439, USA

Leopold Barleon
Kernforschungszentrum Karlsruhe
GmbH, IATF, Postfach 3640, W-7500
Karlsruhe 1, Federal Republic of
Germany

Keiji Miyazaki
Department of Nuclear Engng,
Faculty of Engng, Osaka University
Yamadaoka 2-1, Suita-shi, Osaka,
Japan, 565-0

MS 316

July 1994

The submitted manuscript has been authored by a contractor of the U. S. Government under contract No. W-31-109-ENG-38. Accordingly, the U. S. Government retains a nonexclusive, royalty-free license to publish or reproduce the published form of this contribution, or allow others to do so, for U. S. Government purposes.

DISCLAIMER

This report was prepared as an account of work sponsored by an agency of the United States Government. Neither the United States Government nor any agency thereof, nor any of their employees, makes any warranty, express or implied, or assumes any legal liability or responsibility for the accuracy, completeness, or usefulness of any information, apparatus, product, or process disclosed, or represents that its use would not infringe privately owned rights. Reference herein to any specific commercial product, process, or service by trade name, trademark, manufacturer, or otherwise does not necessarily constitute or imply its endorsement, recommendation, or favoring by the United States Government or any agency thereof. The views and opinions of authors expressed herein do not necessarily state or reflect those of the United States Government or any agency thereof.

Paper presented at the 3rd International Symposium on Fusion Nuclear Technology, Los Angeles, CA, June 27-July 1, 1994

*Work supported by the U.S. Department of Energy, Office of Fusion Energy, under Contract W-31-109-Eng-38.

MASTER

DISTRIBUTION OF THIS DOCUMENT IS UNLIMITED 870

PRESENT UNDERSTANDING OF MHD AND HEAT TRANSFER PHENOMENA FOR LIQUID METAL BLANKETS

Igor R. Kirillov
D. V. Efremov Scientific Research
Institute of Electrophysical
Apparatus, 189631 St. Petersburg,
Russia

Claude B. Reed
Fusion Power Program
Technology Development Division
Argonne National Laboratory
Argonne, IL 60439, USA

Leopold Barleon
Kernforschungszentrum Karlsruhe
GmbH, IATF, Postfach 3640, W-7500
Karlsruhe 1, Federal Republic of
Germany

Keiji Miyazaki
Department of Nuclear Engng,
Faculty of Engng, Osaka University
Yamadaoka 2-1, Suita-shi, Osaka,
Japan, 565-0

Abstract

A review of experimental work on magnetohydrodynamic (MHD) and heat transfer (HT) characteristics of liquid metal flows in fusion relevant conditions is presented. Experimental data on MHD flow pressure drop in straight channels of round and rectangular cross-section with electroconducting walls in a transverse magnetic field show good agreement with theoretical predictions; and simple engineering formulas are confirmed. Less data are available on velocity distribution and HT characteristics, and even less data are available for channels with electroinsulating walls or artificially made self-healing electroinsulating coatings. Some experiments show an interesting phenomena of HT increase in the presence of a transverse or axial magnetic field. For channels of complex geometry — expansions, contractions, bends, and manifolds — few experimental data are available. Future efforts should be directed toward investigation of MHD/HT in straight channels with perfect and nonperfect electroinsulated walls, including walls with controlled imperfections, and in channels of complex geometry. International cooperation in manufacturing and operating experimental facilities with magnetic fields at, or even higher than, 5-7 T with comparatively large volumes may be of great help.

1. Introduction

Liquid metals (LM) are considered as prospective coolants in many designs of fusion reactor blankets and divertor targets [1-7]. For blanket applications LM flow is generally channel flow, whereas it may be either channel flow or a free surface flow (films, jets or droplets) for divertor applications. Here, we confine ourselves to channel flow.

The motion of LM in a strong magnetic field generally induces electric currents, which, while interacting with the magnetic field, produce electromagnetic forces that change the velocity distribution and turbulent pulsation characteristics and exhibit an integral retarding force on the flow. These effects change heat-transfer characteristics, pressure drop, and the required pumping power for the cooling system from those of the case where no magnetic field is present (for example, in fast breeder reactors). Therefore, the knowledge of LM MHD/HT flow characteristics under fusion relevant conditions is one of the key issues in making an optimal design for fusion reactor LM cooling/tritium breeding systems, and in estimating their prospects.

LM systems of fusion reactors are characterized by high values of MHD and hydrodynamic flow parameters: Hartmann number $M=2 \cdot 10^3 - 1 \cdot 10^5$; Reynolds number $Re=1 \cdot 10^4 - 6 \cdot 10^5$; Interaction parameter $N=40 - 5 \cdot 10^4$; Peclet number $Pe=300 - 1 \cdot 10^4$. Such LMs as Li, Li₁₇Pb₈₃, and Pb are considered for blanket applications, while Li, Ga, Na are considered for divertors. There are quite a number of publications on theoretical and experimental investigations of such flows, in spite of some attempts [8,9,10] though, organization of this knowledge is

still necessary. An attempt is made here to summarize the results of MHD/HT studies in fusion relevant LM flows conducted in different countries. Channel flows and the following other configurations are considered: straight ducts of constant and variable cross-section, elbows, bends, and manifolds.

2. MHD Flow In Straight Channels Under Transverse Magnetic Field

2.1 Constant Area Cross Section Channels In Transverse Uniform Magnetic Fields

This type of flow is most often studied, both theoretically and experimentally. A summary of these studies at moderate values of M and N ($N < 10$) may be found in [8,11], whereas all experimental data known to the authors, at conditions of $M \gg 1, N \gg 1$ is discussed here (see Table 1).

From theoretical analysis it follows that under $M \gg 1, N \gg 1$ the flow in conducting wall ducts consists of the core, where the pressure gradient is counterbalanced by the electromagnetic force and velocity is nearly constant; and two near-wall layers: the Hartmann layer with a thickness of the order of M^{-1} near the walls which are perpendicular to the magnetic field and the sidewall layer with a thickness of the order of $M^{-1/2}$ near the walls which are parallel to the magnetic field. The flow structure strongly depends on the channel aspect ratio b/a (see Fig. 1), the wall conductance ratio $c = \sigma_w t_w / \sigma L$, and the electrical resistance of the electroinsulating film, if any. For all mock-ups of Table 1, where $c \gg M^{-1}$ (except those with $c=0$), simple engineering formulas for pressure drop hold true.

Experimental results for the pressure gradient (its absolute value) in channels with electroconducting walls may be expressed as follows:

$$dp/dx = k_p \sigma U_0 B_0^2 \quad (1)$$

with experimental values of k_p shown in Table 2.

A number of simple analytical expressions are available for k_p . Under conditions of large M these expressions reduce to the following ones:

$$k_p = c/(1+c) \quad (2)$$

for round ducts, Miyakzaki et al. [13], where

$$c = \sigma_w (r_o^2 - r_i^2) / \alpha (r_o^2 + r_i^2) \quad (3)$$

and

$$k_p = c/(1+a/3b+c) \quad (4)$$

for rectangular ducts [16,19,22], where

$$c = \sigma_w t_w / \sigma a \quad (5)$$

Expression (3), under the condition of $t_w/r_i = (r_o - r_i)/r_i \ll 1$, reduces to $c = \sigma_w t_w / \sigma r_i$, which is analogous to (5) with r_i as the characteristic length.

In some papers, the pressure drop in such flows is expressed through hydraulic resistance as in classical hydrodynamic flows:

$$dp/dx = \lambda \rho U_0^2 / 2L \quad (6)$$

From (1) and (6) one can derive

$$\lambda = 2k_p N. \quad (7)$$

For a rectangular channel with walls of different thicknesses and/or conductivities, the following expression is derived for k_p , Hua et al. [21]:

$$k_p = [1 + c^{-1} + (a/6b) \cdot (c_1^{-1} + c_2^{-1})]^{-1}$$

where c is the conductance ratio of walls at $y=\pm a$, and $c_{1,2} = \sigma_{w1,2} t_{w1,2} / \sigma a$ are the conductance ratios of walls at $z=\pm b$ (see Fig. 1). Its comparison with experimental values is shown in Table 2 for channel 17.

In principle, there are numerical solutions (see for example Hua et al. [21]) that can treat the flow in channels with wall conductance ratio arbitrarily changing along the cross-section and length, but few experiments are available to check them. For rectangular ducts (14 in Table 1) with one thick sidewall and three thin walls separated by electrical insulation from thicker, back-up walls, numerical results for the pressure gradient are 10-25% lower than experiments. The 10% figure corresponds to tests under laminarized flow conditions with no velocity pulsations.

Experimental data for velocity profiles in constant area ducts are rare due to difficulties of measurements in liquid metal MHD flows and because of the small cross-sections used. A comparison of measured and calculated velocity profiles in the z-direction for channels 12 and 14 of Table 2 is shown in Fig. 2. Experimental data for channel 12 were obtained by measuring the potential difference between a movable point electrode and a stationary one on a sidewall, whereas the data for channel 14 was acquired by measuring the potential difference between two movable electrodes spaced 1.5 mm apart (LEVI probe). Calculations for Fig. 2 are based on solutions from Sidorenkov et al. [23]. At a given set of parameters, the larger deviations between theory and experiment in the side wall layer for channel 14 may be attributed to velocity fluctuations in this sidewall layer (see below). Different values for velocity peaks in the sidewall layers of this channel are due to different sidewall thicknesses, the peak being smaller near the thicker wall.

Several ideas were proposed for MHD pressure drop reduction, which result in the decrease of mechanical stresses in duct walls and pumping power. One idea is to use high aspect ratio channels oriented with the longer side of the cross section parallel to the magnetic field, the so-called slotted channel, Lavrent'ev [9]. The reduction of the dimensionless pressure drop, k_p , with increasing ratio a/b can be clearly seen in expression (4) and in experimental data from channels 8, 10, and 11 of Tables 1 and 2, which have the same wall thicknesses, $t_w = 2.1$ mm, but different values of a/b . This positive result must be weighed against the increase of heat transfer non-uniformity in comparison with square ducts, an effect which is especially pronounced for conducting walls.

As the ratio a/b increases, the mechanical stresses in the side walls also increase, but at a rate faster than the pressure drop decreases. Therefore, the

introduction of anchor links — cylindrical rods, placed over the channel axis, and bracing the side walls — was proposed. This, of course, will lead to a pressure drop increase compared with the no anchor link case, and to a side wall temperature rise near the links due to the decrease in velocity behind them. Experiments (12 and 14 in Table 1) revealed that the pressure drop increased by a factor of 1.5-1.8 for the following anchor link geometry: relative rod diameter - $d/2a=0.2$ (channel 12) and $d/2a=0.11$ (channel 14); relative distance between rods - $h/d=5$ (channel 12) and $h/d=9.3$ (channel 14). Heat transfer characteristics with anchor links are discussed in the last section of the paper.

Another proposal for pressure drop reduction is the use of thin walls, electrically insulated from thick back-up walls that withstand the mechanical stresses, or sandwich type flow channel inserts (FCI), Malang et al. [24]. As is seen from (1) - (5), the pressure gradient is proportional to wall thickness under the condition $c \ll 1$ which is usually the case for fusion blankets. Experimental results (5 and 14 in Tables 1 and 2) show a drastic decrease in the pressure drop or k_p with the use of 0.5-mm inserts in the first channel, and three 1-mm thick walls, insulated from back-up walls in the second channel.

A radical way to decrease the MHD pressure drop is to use an insulated wall channel, with a self-healing electroinsulating coating on the channel walls (for example Malang et al. [43]). The self-healing coatings do not give perfect electrical insulation with a large specific resistance, but hopefully large enough to ensure the desired decrease in pressure drop.

There are quite a number of experimental data [8,11] on MHD flow in channels with walls of perfect and high electrical resistance ($\sigma_w/\sigma \approx 10^{-18}$) but with characteristic parameters far from the range used in fusion application ($M < 1000$,

$N < 1.5$). In these experiments under a laminarized flow regime, the pressure gradient is proportional to U_0 and B and may be calculated with the following asymptotic formula obtained by Shercliff [25,26]:

for rectangular channels

$$\lambda = 2 M / \text{Re} \cdot (1 - 0.852 / (M^{1/2} \beta) - M^{-1})^{-1}, \quad (8)$$

for round pipes

$$\lambda = 3\pi M / 4 \text{Re} \cdot (1 - 3\pi / 2 M)^{-1}, \quad (9)$$

where $\beta = b/a$ and the characteristic length $L = a$ or $L = r_i$ for rectangular and round ducts, respectively.

Formula (8) gives good agreement with experiments when $M^{1/2} \beta > 5$ (the range for β in experiments is $0.07 < \beta < 50$). A laminarized flow regime takes place when $M/\text{Re} > 4 \cdot 10^{-3}$. For round channels, formula (9) is applicable with good accuracy at $M \geq 10$ but there is no single critical number $(M/\text{Re})_{\text{crit}}$ for transition from a turbulent to laminarized flow regime. This critical number decreases as Re increases. To be on the safe side, one can assume $(M/\text{Re})_{\text{crit}} = 5 \cdot 10^{-3}$ when $\text{Re} \geq 1 \cdot 10^5$.

Velocity profile measurements in these experiments show a flatter profile than in the non-magnetic field case.

In the range of characteristic parameters that are of interest for fusion applications ($M \gg 1$, $N \gg 1$), there are very few experimental data (7, 12, 15, and 16 in Table 1) and they are only for pressure drops. Rectangular channel results show only qualitative agreement with theory: formula (8) can not be applied to channel 16 in Table 1, since $\beta M^{1/2} = 1.1-1.2$ and is beyond the range of the formula's applicability; for channel 15 in Table 1 the authors of [18] attribute the discrepancy between theory and experiment to additional Hartmann flow friction in duct corners due to excessive epoxy bond layers.

Inclination of the transverse magnetic field with respect to the channel side wall (θ in Fig. 1) increases hydraulic resistance but at a slower rate than predicted by theory, Molokov et al. [27]. (See Fig. 3 for channel 16 in Table 1.) The reason for this discrepancy between theory and experiment may be attributed to the small value of $\beta M^{1/2}$ in the experiment and the $M \rightarrow \infty$ assumption of the theory. For channel 12 in Table 1, the experimental value of $\lambda(\theta = 24.6^\circ)/\lambda(\theta = 0)$ is equal to 1.7, while theoretical predictions give 1.4.

For a round duct with insulated walls (7 in Table 1), the experimental value of λ is fairly close to the theoretical one (9), exceeding it by less than 17%.

2.2 Constant Area Cross-Section Channels in Transverse Nonuniform Magnetic Field

Changing the transverse magnetic field over the duct length gives rise to an axial potential difference which drives currents in the axial direction, the circuit being closed by the walls or/and the side layers. These currents, while interacting with the magnetic field, produce electromagnetic forces which drive the fluid out

of the core and into the regions near the side walls. This also results in a higher MHD pressure drop than in a uniform magnetic field.

Experimental data for round and rectangular ducts with electroconducting walls (6,13 in Table 1) are compared with a 3-D code in Figs. 4 and 5. Velocities (Fig. 4) are measured again with a LEVI probe. The transverse pressure difference (difference between pressures at two points 90° apart in one cross-section — see [17,21]) is a nice measure of 3-D effects and is equal to zero in a uniform magnetic field (the fringing field zone is $-5 < x/L < +5$). It is worth mentioning that the 3-D ANL code based on non-inertial, non-viscous flow equations and valid for $M \gg 1, N \gg 1$, gives good agreement with experiments under as low values of M and N as $N=540$ and $M=2900$.

The MHD pressure drop in the whole region of the fringing field may be obtained by integrating data of Fig. 5 over the duct length. In some cases where the relative rate of change in the magnetic field is small, i.e.,

$$dB/dx \cdot L/B_0 \approx \Delta B/B_0 \cdot L/x_0 \ll 1, \quad (10)$$

pressure drop may be calculated with the following simple formula:

$$\Delta p = \Delta p_{fd} = \int_{x_2}^{x_1} (dp/dx) dx \quad (11)$$

where dp/dx is calculated according to (6) with λ from (7) for electroconducting walls or from (8,9) for electroinsulating walls. Discrepancy between values

calculated in this way and experimental data for channels 1,8,9,10,11 of Table 1 is less than 10% with $5 < x_0/L < 15$.

It should be noted that (11) gives good correlation with experimental data, when (10) holds true, but only in an integral way (for the whole nonuniform field region); the formula may show some discrepancy for local dp/dx dependence.

By using (11) we neglect 3-D effects. In general, for the dimensionless pressure drop, the following expression is obtained in Hua et al. [21]:

$$\Delta\bar{p} = \Delta p / (\sigma U_0 B_0^2 L) = \Delta\bar{p}_{fd} + \Delta\bar{p}_{3-D} , \quad (12)$$

where $\Delta\bar{p}_{fd}$ is calculated according to (11) for locally fully developed flow and $\Delta\bar{p}_{3-D}$ represents 3-D effects. In a square duct with equal wall conductance ratio and normalized $B(x)$ as follows:

$$B(x) = \begin{cases} 1 & x \leq -x_0 \\ 0.5(1 - \sin(\pi x / 2x_0)) & -x \leq x \leq x_0 \\ 0 & x \geq x_0 \end{cases}$$

$\Delta\bar{p}_{3-D} = k_{3-D} C^{1/2}$ for $C < 0.1$ and the following values of k_{3-D} vs. x_0/L were determined:

| k_{3-D} | x_0/L |
|-----------|---------|
| 0.158 | 2 |
| 0.126 | 3 |
| 0.105 | 4 |

From experiments (6,13 in Table 1) it was found that $k_{3-D} = 0.18$ for a round duct and $k_{3-D} = 0.13$ for a rectangular one ($x_0/L=5$).

For channels with electroinsulating walls in nonuniform magnetic fields, the pressure drop reveals the transition from viscous to non-inertial non-viscous flow, where the normalized pressure drop $\zeta/N = \Delta p / (\rho U_0^2/2)N$ depends only slightly on N (see Fig. 6a for channel 16 in Table 1). Quite a distinct boundary is found between these two regimes (Fig. 6b), with $\zeta = \zeta_0 + \zeta_1 M/Re$ in the region where viscous forces prevail and $\zeta = \zeta_2 M^2/Re$ in the region where electromagnetic forces prevail (so called linear type of flow). By plotting experimental data as $\zeta = f(M/Re)$ for different values of $M=const$, one can easily obtain boundary curves of the transition from viscous to linear type flow (Fig. 6b). For a different magnetic field inclination angle θ , all data can be put on one boundary curve (Fig. 7a) using the following characteristic length in the M and N parameters:

$$\begin{aligned} L &= b/\sin \theta & \tan \theta > b/a, \text{ or} \\ L &= a/\cos \theta & \tan \theta \leq b/a. \end{aligned}$$

To the right of this curve the flow is linear (non-inertial), to the left it is viscous. In the viscous flow regime ζ_1 is a function of θ only, and the dependence of $\zeta_1 = f(\theta)$ is qualitatively the same as for $\lambda = f(\theta)$. Here the pressure drop in the nonuniform magnetic field, if (10) is fulfilled, may be calculated under the assumption of locally fully developed flow (11). Results of such a calculation is shown in Fig. 3.

In the linear flow regime $\zeta_2 = k_1 M^{-1/2} + k_0$, which corresponds to the asymptotic estimation made in Hunt and Shercliff [28].

For a round duct (7 in Table 1) the pattern of transition from viscous to linear-type flow is also clearly seen, but unfortunately no data are available for replotting the curves and obtaining the border line as was described earlier.

2.3 Channels of Variable Cross-Section in a Uniform Magnetic Field

The fact that increased velocity near side walls in MHD flows has been demonstrated, gives rise to several ideas for velocity distribution control, Walker and Picologlou [29]. Velocity increases near the blanket first wall with high heat flux could lead to HT enhancement, the decrease of mean flow velocity, keeping the same allowable maximum wall temperatures; and a net pressure drop reduction. HT enhancement may result from higher than average flow velocity in the near wall jet, near wall velocity fluctuations, and non-zero transverse velocity components (in some geometries). At least three ideas for actively influencing the velocity distribution (flow tailoring) have been proposed: (1) an increase in the electrical resistance of the heated wall parallel to the magnetic field by decreasing its thickness; (2) an electrical resistance and/or thickness variation of Hartmann walls in such a way as to increase the flow rate near the first wall; and (3) an axial variation of duct cross-section dimensions in such a way that it consists of a series of expansions and contractions with sections of constant area between them (expansion and contraction cross-sections may be of trapezoidal or rectangular type).

So far there are few experimental data to verify any theoretical predictions. In an experiment, Picologlou et al. [30,31], which utilizes two of these ideas, potential distribution and limited data for velocity measurements are available. Nevertheless they clearly demonstrate the following (Fig. 8):

- a. the velocity near the thin wall ($t = 1.5\text{-mm SS}$ at $z/L = -1$) is distinctly larger than that near the thick wall ($t_w = \{4\text{-mm copper} + 6\text{-mm SS}\}$ at $z/L = +1$);
- b. the near wall jet velocity is higher in the middle of an expansion than in a constant area section of the duct;
- c. 3-D code predictions for non-inertial, non-viscous flow are in good agreement with experimental data; and
- d. high velocity fluctuations are observed in the near wall jet.

3. MHD Flows in Ducts of Complex Geometry

In blanket and divertor target designs, apart from straight ducts, more complex geometries are used: confusers/diffusers, bends, turns, and manifolds. MHD flow in all of these ducts is characterized by an axial electric potential difference giving rise to the same effects as in the case of the nonuniform magnetic field described above. The drag coefficient ζ decreases as N increases due to suppression of inertial effects by the magnetic field and reaches some asymptotic value which is independent of N . The value of N , starting from $\zeta/N = \text{const}$, depends in general on the duct geometry and Hartmann number.

For all experiments performed (see Table 3) the dependence of $\zeta/N = f(N)$ qualitatively corresponds to that of Fig. 6a. The transition boundary from inertial to non-inertial flow in M-N coordinates and asymptotic values of $(\zeta/N)_{as} = \Delta p / (\sigma U_0 B_0^2 L)$ are shown in Figs. 9 and 10 for the flows of Table 3, where such information is available. The characteristic length L for every channel is shown in Table 3 as well. One should treat the boundary curves as approximate since they are obtained from experimental data analogous to that of Fig. 6a and not from the curves of $\zeta = f(M/Re)$ as described above for insulated ducts in a transverse nonuniform magnetic field.

From Fig. 9, $N_{crit} \approx 4 \cdot 10^3$ ($\lg N_{crit} \approx 3.6$) for channels 4, 5, 6, and 8 and $N_{crit} \approx 1 \cdot 10^4$ for channel 3. All channels have electroconducting walls, except for channel 6. None of these N_{crit} values depends on M, however, N_{crit} does depend on M, for channels 9 and 10 (with electroinsulating walls). To the left and/or up from boundary curves lies the region of non-inertial flow, whereas to the right and/or below the curves lies the region of non-inertial flow.

Asymptotic values of ζ/N for channels 3, 4, 5, 6, and 8 depend on M only slightly, while they are proportional to $M^{-1/2}$ for channels 9 and 10 [$(\zeta/N)_{as}$ for channel 10 varies from 4.0 for $M=651$ to 5.6 for $M=175$ and is not shown in Fig. 10]. To compare all these values of $(\zeta/N)_{as}$ one has to keep in mind that they represent a pressure drop in elements perpendicular to the magnetic field as well as 3-D effects resulting from flow direction change:

$$(\zeta/N)_{as} = \Delta p_{fd} / (\sigma U_0 B_0^2 L) + (\zeta/N)_{3-D}$$

Excluding the first term which corresponds to fully developed flow in straight channels with length ℓ in a transverse magnetic field, i.e.

$$\frac{\Delta p_{fd}}{\sigma U_0 B_0^2 L} = \begin{cases} \ell/L \cdot (1 + a/3b + c) & \text{in rectangular ducts} \\ \ell/L \cdot c/(1 + c) & \text{in round ducts ,} \end{cases}$$

one gets the following results for (ζ/N) in one right angle turn (for non-inertial flow, Z and U-bends may be treated as two right angle turns).

For channel 3, the value of $(\zeta/N)_{3-D} = 3.38 \cdot 10^{-2}$ is fairly close to the theoretical one, $(\zeta/N)_{3-D} = 1.063c/(4/3+c) = 4.2 \cdot 10^{-2}$, obtained in Reimann et al. [37] for a core flow solution. This value gives a pressure drop due to 3-D effects in a right angle turn corresponding to that of a straight channel with a relative length $\ell/a=0.853$, which is not too excessive for blanket applications. For channel 11, $(\zeta/N)_{3-D} = 3.9 \cdot 10^{-2}$ (in case of one channel), but the value was obtained for $N=3000$ which is considerably less than N_{crit} . The asymptotic $(\zeta/N)_{as}$ should be less than that, which agrees with the fact that the wall parameter in this channel is less than in channel 3. $(\zeta/N)_{as}=3.44 \cdot 10^{-2}$ and $4.78 \cdot 10^{-2}$ for channels 4 and 5, respectively. These values should be treated with care since there are no exact values of ℓ in Grinberg et al. [34] and channel 5 is of rather complex geometry to be treated in such a simple way. Nevertheless, all values of $(\zeta/N)_{as}$ are of the same order of magnitude and only data for channel 8 falls out of this range.

For channel 9 with electroinsulating walls, after extracting:

$$\Delta p_{fd}/(\sigma U_0 B_0^2 b) \approx \ell/(bM_a) ,$$

where M is calculated using the characteristic length $L=a$, the dependence of $(\zeta/N)_{3-D} = f(M^{-1/2})$ still remains due at least to the same dependence from M for side layer thickness through which longitudinal currents are closed. There is no core flow solution available for comparison with these experimental results.

The following additional information can be derived from the experiments. For calculation of ζ in a right angle, smooth turn of round channel with insulated walls and $N>10$ (in the inertial-viscous flow regime), the following empirical expressions are recommended.

$$\zeta = k_2 3\pi M / 2 \text{Re} \cdot (1 - 3\pi M)^{-1} \cdot R / 2d$$

-for B perpendicular to the plane of turn with $k_2=1.05-1.15$; and

$$\zeta = k_3 N$$

-for B parallel to the plane of turn with $k_3=0.125$.

The drag coefficient is larger for B parallel to the plane of the turn than for B perpendicular, which corresponds to predictions of Molokov [38]. This conclusion has a general meaning — any change of cross-section in a plane parallel to B leads to more pronounced 3-D effects than in the plane perpendicular to B .

Measurements of wall potential difference, which may be interpreted as local velocities averaged over the channel height, in mock-ups 1 and 2 (Table 3), show the suppression of inertial effects with increasing N . In a right angle turn under a weak magnetic field, the flow is strongly nonuniform with maximum

velocity near the rear wall as noted in Table 3. With N increasing, the velocity distribution becomes more symmetrical; electroconducting side walls stimulate this process.

In model 2 (Table 3), for a region of sharp cross sectional change, the magnetic field suppresses velocity vortices, but they are still present under the highest $N > N_{crit}$ value reached. This means that non-inertial flow (from an integral point of view) is still inertial when we are considering its local characteristics.

Concluding this part we should point out that data for ducts of complex geometry are not as numerous as for straight ducts and they are mainly for pressure drop and side wall potential distribution. The few experimental data on velocity distribution in such types of flows recently published, Reimann et al. [45], show that at higher N the liquid is preferentially flowing close to the side wall and a pair of strong vortices is generated at the entrance of the branch parallel to the magnetic field. Both of these effects are favorable for heat transfer. Therefore, more experimental and theoretical work are needed to confirm these effects and develop empirical correlations analogous to those in ordinary hydrodynamics.

3.1 Flows in Manifolds

Two experiments are known to the authors on this type of flow (channels 10 and 11 in Table 3). In the first one, the flow from a round pipe ($d=26$ mm) oriented along the magnetic field is distributed in 5 smaller pipes ($d=10$ mm) placed perpendicular to the magnetic field and then goes to another $d=26$ mm pipe aligned with the magnetic field. The small pipes do not have electrical contact

with each other except through the inlet/outlet. Drag coefficient behavior in this U-bend was discussed earlier. Flow rate distribution over the small parallel pipes becomes more uniform with increasing N — the root mean square of flow deviations D is decreasing. The asymptotic value of D is reached when N is approximately 10 times less than that giving the asymptotic values for ζ/N . Another important result is that the asymptotic value of D is growing with increasing M : $D \approx 8\%$ for $M=90$ and $D \approx 20\%$ for $M=340$.

In the second experiment, from 1 to 5 channels of square cross section form a U-bend from the perpendicular to parallel direction with respect to the magnetic field. When individual channels are electrically connected, the multichannel effect (MCE) takes place, which means that currents induced in one channel can flow through the others changing the flow distribution in them.

When an equal pressure drop is applied to all channels, the flow rates in the individual channels Q_i are distributed in such a way that their values in the outer channels become significantly larger than those in the inner channels as N increases. The asymptotic values of Q_i/Q (independent of N) are reached at $N \approx 1000$ and equal to 0.285-0.3 for outer channels, 0.12 - for the inner channel and 0.15 for the other two. The MCE is more pronounced for nonconducting outside walls than for conducting ones, since in the first case more current in the side layers of the outer channels is forced to flow parallel to the magnetic field thus allowing a higher flow rate in these layers.

For a constant flow rate mode ($Q_i = \text{const}$) pressure drops in the channels become unequal with the reverse pattern — the lowest one in the outer channels and the largest in the inner ones. For every channel, the drag coefficient (dimensionless

pressure drop) decreases with increasing N but does not reach an asymptotic value up to $N=5 \cdot 10^4$ obtained in the experiment. So pressure drops in individual channels as predicted by the Core Flow Approximation (valid for $N \rightarrow \infty$) are significantly less than those in experiments, though their ratio agrees well with experimental results.

A radical way of significantly reducing MCE and obtaining an equal flow rate distribution in multichannel flow is to electrically decouple individual channels in sections where the flow is perpendicular to the magnetic field. This was successfully demonstrated by an experiment using the FCI technique. Flow rate deviations in individual channels was less than 8% from the average value.

4. Heat Transfer In Liquid Metal MHD Flow

Many experiments were carried out in previous years on heat transfer in liquid metal forced flow under axial and transverse magnetic fields in the following range of characteristic parameters: $1 \cdot 10^3 < Re < 1 \cdot 10^7$; $M < 1200$; $N < 160$; $0.01 < Pr < 0.05$; $1 \cdot 10^2 < Pe < 5 \cdot 10^3$. From these experiments it follows that the axial magnetic field suppresses turbulent pulsations although not enough to substantially influence the average velocity profile. This leads in general to a decrease of heat transfer characteristics (Nusselt number Nu) with increasing magnetic field or M . Since $Nu = Lq/\eta(T_w - T_b)$, its decrease under a given heat flux means an increase in the temperature difference between the wall (T_w) and the liquid metal bulk flow (T_b). The critical Re for transition from laminar to turbulent flow, increases, when an axial magnetic field is applied.

A transverse magnetic field changes the velocity distribution in channels and suppresses turbulent pulsations. The first effect may lead to heat transfer enhancement due to large velocity gradients near the walls. But in general it follows from previous experiments that the Nu decreases due to pulsation suppression when M increases .

Some recent work (see Table 4) revealed a number of new effects that are considered briefly here.

For a vertical lithium flow in an annular channel (channel 1, Table 4) placed in an axial magnetic field and heated with a uniformly distributed flux on the inner tube, an unexpected increase of Nu in the magnetic field was observed. Under $Re=const$ with B or M increasing, Nu decreases, at first, from its value at $B=0$, which is consistent with previous results. This decrease is small (about 17%) at $Re=(2.5-5) \cdot 10^3$ and takes place with $M < 360$, amounts to 50% at $Re=(1-2) \cdot 10^4$ with $M < 700$, and to 70% at $Re=(3-4) \cdot 10^4$ with $M < 1400$.

With further increase of M at $Re=const$, an increase of Nu was observed. At $Re=2.5 \cdot 10^3 - 2 \cdot 10^4$ the increase was so significant that Nu at $M=3600$ (the highest reached) was even higher than its value at $B=0$. The largest value of $Nu=22$ exceeded by 2.75 times $Nu=8$ at $B=0$ with $Re=1 \cdot 10^4$. At $Re=(3-4) \cdot 10^4$ an increase of Nu was observed with $1400 < M < 3600$ but only in comparison to the minimum Nu value at $M=1400$, this increased value still being 2-2.3 times less than the one at $B=0$. There is no good explanation so far for the observed phenomena. It cannot be attributed to the buoyancy forces, as discussed next, since the flow was in the upward direction.

In vertical downward heated mercury flow in an axial magnetic field (channel 2, Table 4), the combined effect of buoyancy forces and the magnetic field on heat transfer intensification was observed. Without the magnetic field, no dependence of Nu on heat flux (Rayleigh number Ra) was observed in the investigated range of Ra values (Fig. 11). With an applied magnetic field, however, Nu monotonically increased with increasing Ra at $M=\text{const}$, approaching its value at $M=0$. Temperature and velocity pulsations (Fig. 12) also increased with Ra/Re . At the same time, suppression of high frequency oscillations and intensification of low frequency ones took place with increasing M . Temperature profiles across the radius with an applied magnetic field and small values of Ra/Re were somewhat stretched, resulting in a decrease of Nu compared with the $M=0$ case. With Ra/Re increasing, the temperature profiles became more flat, as in turbulent flow, and lead to an Nu increase. The effect was most pronounced at $Re/M=30$ where full laminarization of the flow is expected in an axial magnetic field. This additional flow turbulization and heat transfer enhancement is believed to be due to the combined effect of buoyancy forces (counter thermogravitational convection) and the longitudinal magnetic field.

The first experimental results with the same tube in an axial, horizontal magnetic field also revealed influences due to buoyancy forces. Distributions of temperature and Nu over the tube circumference are not uniform even when heat flux was uniform, the non-uniformity being increased with an axial magnetic field increase.

For annular flow in a transverse magnetic field (channel 3, Table 4) Nu decreases on the whole with increasing M and approaches a value predicted from the electromagnetically laminarized flat flow velocity model, for which, in this case,

$Nu=Nu_{\ell}=6.38$. In Fig. 13 the ratio of Nu excess over the laminarized value Nu_{ℓ} in the presence (Nu^*) and absence (Nu) of a magnetic field:

$$\bar{Nu} = (Nu^* - Nu_{\ell}) / (Nu - Nu_{\ell})$$

is shown, as well as the normalized RMS value of temperature pulsations in the LM at the same cross section, as a function of M^2/Re . Large deviations from the monotonic decrease of \bar{Nu} with increasing M^2/Re may be seen near $M^2/Re=1$ and this region corresponds to maximum fluctuations in the flow. The singular rise of \bar{Nu} is considered to be the result of enhanced local turbulence due to large velocity gradients near the heater pin wall where the MHD forces are high.

For rectangular channel flow in a transverse magnetic field with heat flux applied to one side wall (channel 4, Table 4), unfortunately only a limited amount of data is available. The following conclusions may be drawn from these tests. At $Pe \approx 200 = \text{const}$ ($Re \approx 8300 = \text{const}$) temperature profiles in the direction perpendicular to the magnetic field become more flat with B increasing from 0 to 2 T (M from 0 to 800). This means that heat transfer is improved and Nu increases from $Nu \approx 5.5$ at $M=0$ to $Nu \approx 8$ at $M \approx 800$ and $N \approx 250$, and to $Nu \approx 11.5$ at $M \approx 800$ and $N \approx 120$. For this particular geometry, the improvement comes mainly from velocity fluctuations in MHD side layer near the heated wall, Evtushenko et al. [44].

Under the conditions of laminar flow and no side layer fluctuations, good correlation exists between 3-D theory and measurements of temperature distribution inside the flow and at the heated wall (Fig. 14). Temperature is normalized by qL/η .

Experiments with anchor links in part of the channel (see above for anchor links description) revealed the following. Temperatures over the channel centerline, where anchor links are situated, are consistently higher than without the links. This effect is more pronounced at lower Pe or Re. There are also perturbations due to 3-D effects associated with the beginning of the anchor link region. In the remainder of the channel other diverse effects of anchor links were not found.

An interesting avenue for heat transfer enhancement is the generation of strong anisotropic large-scale quasi turbulent disturbances in strong magnetic fields using turbulent promoters, Branover and Henoch [42]. An increase of Nu around 1.5 times its value at $B=0$ was demonstrated in rectangular duct mercury flow while inserting a grid upstream of the heat transfer region, with bars parallel to the magnetic field. This is obviously the main method of heat transfer enhancement in channels with electroinsulating walls and it needs further investigation to estimate the penalty for the promotion of turbulence.

5. Conclusion

Existing experimental data and theoretical models allow for the conservative calculation of most of the MHD and heat transfer characteristics of liquid metal flows relevant to fusion blankets. Future efforts should be directed to enlarging our knowledge of MHD/HT phenomena in straight channels with perfect and nonperfect electroinsulated walls and in channels of complex geometry. Upcoming new phenomena, like the heat transfer enhancement from the side wall due to turbulence promotion in thin walled and electrically insulated ducts, open new prospects to self-cooled liquid metal fusion blankets. Therefore, experiments

should be performed at higher values of characteristic parameters so as to simultaneously satisfy all fusion relevant conditions. This requires facilities with magnetic fields at, or even higher than, 5-7 T having comparatively large volumes. International cooperation in constructing and operating of such facilities may be of great help.

Nomenclature

| | |
|----------|--|
| a | channel half width |
| b | channel half height |
| B | magnetic flux density |
| c | wall conductance ratio |
| d | inner cut diameter |
| k | coefficient |
| l | length of channel, magnet or heater |
| L | characteristic length |
| M | Hartmann number ($M=BL\sqrt{\sigma\mu}$) |
| N | interaction parameter ($N=B^2 L\sigma/\rho U_0$) |
| Nu | Nusselt number |
| p | pressure |
| Pe | Peclet number ($Pe=U_0L/\alpha$) |
| r | duct radius |
| R | curvature radius |
| t | thickness |
| T | temperature |
| q | heat flux |
| Q | volume flow rate |
| U | flow velocity |
| x,y,z | Cartesian coordinates |
| α | thermal diffusivity |
| β | channel aspect ratio |
| ζ | pressure drag coefficient |
| η | thermal conductivity |

| | |
|-----------|----------------------------------|
| θ | magnetic field inclination angle |
| λ | hydraulic resistanse |
| μ | dynamic viscosity |
| ν | kinematic viscosity |
| ρ | density |
| σ | electrical conductivity |

Subscripts

| | |
|--------|-------------------|
| as | asymtotic |
| b | bulk |
| crit | critical value |
| fd | fully developed |
| i | inner |
| ℓ | laminar |
| o | outer |
| w | wall |
| 0 | fixed value |
| 3D | three-dimensional |

References

- [1] Blanket comparison and selection study. Final Report, ANL/FPP-84-1(1984).

- [2] B. Picologlou. Self-cooled lithium blanket for ARIES-II, in: Workshop on Liquid Metal MHD. ed. U. Muller (IATF.KfK, 1992).

- [3] E. Muraviev, A.A. Borisov, A.V. Kashirskiy, S.A. Moshkin, P.V. Romanov, et al. Lead cooled blanket for ARIES-II. USSR-USA-Germany Workshop on Liquid Metal Blankets (St. Petersburg, 1991).

- [4] S. Malang, J. Reimann, H. Sebening, L. Barleon, E. Boguseu, et al., DEMO-relevant test blankets for NET/ITER, KfK report, KfK 4907 (1991).

- [5] S. Malang, E. Bojarsky, L. Bühler, H. Deckers, V. Fischer, et al. Dual coolant liquid metal breeder blanket, in: Proc. 17th Symp. on Fusion Technology, Rome, v. 2. ed. C. Ferro, M. Gasparotto, H.Knoepfel (Elsevier Science Publishers B.V., Amsterdam, 1993) pp. 1424-1428.

- [6] DEMO project. Conceptual design of demonstration fusion reactor DEMO. Kurchatov Institute Report, RSC Kurchatov Institute, Moscow (1993) — in Russian.

- [7] ITER reference blanket-shield design and advanced blanket concept, ITER TAC-4-07 (1994).

- [8] V.A. Glukhikh, A.V. Tananaev and I.R. Kirillov, Magnetohydrodynamics in Nuclear Energetics (Energoatomizdat, Moscow, 1987) pp. 35-43, 63-70.— in Russian.
- [9] I.V. Lavrent'ev. MHD flows at high R_m , N and Ha , in: Liquid Metal Magnetohydrodynamics. ed. J. Lielpeteris and R. Moreau (Kluwer Academic Publishers, Dordrecht/Boston/London, 1989) pp. 21-27.
- [10] B.G. Karasev and A.V. Tananaev, Liquid metal fusion reactor systems, Plasma Devices and Operations 1 (1990) 11-30.
- [11] Yu M. Gelfgat, O.A. Lielausis and E.V. Scherbinin, Liquid Metal Under Electromagnetic Forces (Zinatne, Riga, 1976) pp. 36-50.
- [12] K. Miyazaki, K. Konishi, H. Aoyama, S. Inoue and N. Yamaoka, Reduction of MHD pressure drop of liquid metal flow by insulation. Part 1: Insulated circular ducts, Fusion Technology 19 (1991) 961-968.
- [13] K. Miyazaki, K. S Kotake, N. Yamaoka, S. Inoue and Y. Fujii-e, MHD pressure drop of NaK flow in stainless steel pipe, Nuclear Technology/Fusion 4 (1983) 447-452.
- [14] K. Miyazaki, Y. Shimakawa, S. Inoue, N. Yamaoka and Y. Fujii-e, Flow and heat transfer characteristics in lithium loop under transverse magnetic field, Nuclear Technology/Fusion 4 (1983) 733-738.

- [15] L. Barleon, L. Lenhart, H. Mack, A. Sterl and K. Thomauske. Investigation on liquid metal MHD in straight ducts at high Hartmann numbers and interaction parameters, in: Proc. of the 4th Intern. Topical Meeting on Nuclear Reactor Thermal Hydraulics (Karlsruhe, 1989) pp. 857-862.
- [16] A.Y. Ying and M.S. Tillack. MHD heat transfer in elongated rectangular ducts for liquid metal blankets, 9th Topical Meeting on the Technology of Fusion Energy (Oak Brook, Ill., 1990).
- [17] C.B. Reed, B.F. Picologlou, T.Q. Hua and J. S. Walker, ALEX Results — a comparison of measurements from a round and a rectangular duct with 3-D code predictions, IEEE 12th Symposium on Fusion Engineering (Monterey, California, 1987).
- [18] K. Miyazaki, K. Konishi and Y. Gonno, Reduction of MHD pressure drop of liquid metal flow by insulation. Part II: Three-face insulated rectangular duct, Fusion Technology 19 (1991) 969-975.
- [19] K. Miyazaki, S. Inoue and N. Yamaoak, Magneto-hydro-dynamic pressure drop of lithium flow in rectangular ducts, Fusion Technology 10 (1986) 830-836.
- [20] A.A. Gaizer, I.A. Eutushenko, A.V. Tananaev and Yu P. Tckeinyev, MHD flow in the slotted channels. Experimental results. USSR-USA-Germany. Workshop on Liquid Metal Blankets (St. Petersburg, 1991).

- [21] T.Q. Hua, J.S. Walker, B.F. Picologlou and C.B. Reed, Three-dimensional magnetohydrodynamic flows in rectangular ducts of liquid-metal-cooled blankets, *Fusion Technology* 14 (1988) 1389-1398.
- [22] C.B. Reed, T.Q. Hua, D.B. Black, I.R. Kirillov, S.I. Sidorenkov, et al. Liquid metal MHD and heat transfer in a Tokamak blanket slotted coolant channel, in: *Proc. of IEEE/NPSS 15th Symposium on Fusion Engineering* (Hyannis, MA, 1993) PP. 263-272.
- [23] S. Sidorenkov and A. Shishko, Variational method for MHD flow calculation in conducting walls slotted channels, *Magnetohydrodynamics* 4 (1991) 87-96.
- [24] S. Malang, K. Arheidt, L. Barleon, M.V. Borgstedt, V. Casal, et al., Self-cooled liquid metal blanket concept, *Fusion Technology* 14 (1988) 1343-1356.
- [25] J.A. Shercliff, Magnetohydrodynamic pipe flow. Part II. High Hartmann number. *J. Fluid Mech.* 13 (1962) 513-518.
- [26] J.A. Shercliff, Steady motion of conducting fluids in pipes under transverse magnetic fields, *Proc. Cambridge Philos. Soc.* 49 (1953) 136-144.
- [27] S. Molokov and A. Shishko, Fully developed magnetohydrodynamic flows in rectangular ducts with insulating walls, KfK report, KfK 5247 (October 1993).
- [28] J.C.R. Hunt and J.A. Shercliff, Magnetohydrodynamics at high Hartmann numbers, *Ann. Rev. Fluid Mech.* 3 (1971) 37-62.

- [29] J.S. Walker and B.F. Picologlou, Comparison of three MHD flow control methods for self-cooled liquid metal blankets, *Fusion Technology* 10 (1986) 866
- [30] B.F. Picologlou, C.B. Reed, T.Q. Hua, J.S. Walker, L. Barleon, et al., Experimental investigation of MHD flow tailoring for first wall coolant channels of self-cooled blankets, *Fusion Technology* 15 (1989) 1180-1185.
- [31] B.F. Picologlou, C.B. Reed, T.Q. Hua, J.S. Walker, L. Barleon, et al., MHD flow tailoring in first wall coolant channels of self-cooled blankets, *Fusion Engrg. Des.* 8 (1989) 297-303.
- [32] I.A. Evtushenko, A.T. Kusainov and A.V. Tananaev, Experimental investigation of MHD processes in slotted channel under strong magnetic field, *Magnetohydrodynamics* 2 (1992) 89-100.
- [33] L. Barleon, L. Bühler, S. Molokov, R. Stieglitz, B.F. Picologlou, et al., Magnetohydrodynamic flow through a right angle bend, *Proc. Seventh Beer-Sheva Intern. Seminar on MHD Flows and Turbulence.* Israel. 1993, to appear.
- [34] G.K. Grinberg, M.Z. Kaudze and O.A. Lielausis, Investigation of local MHD pressure drop on sodium loop with superconducting magnet, *Magnetohydrodynamics* 1 (1985) 121-126.
- [35] A.V. Tananaev, T.N. Aitov, V.P. Bocheninskiy, Yu B. Emelin, A.I. Kalutic, et al., Modelling of hydrodynamic processes in liquid metal MHD energy converters, in: *Proc. Eighth Intern. Conf. MHD Electrical Power Generation*, vol.4 (Moscow, 1983) pp. 77-83.

[36] T.N. Aitov, A.V. Tananaev and V.A. Shinatenko, Experimental investigation of MHD flow transition to linear regime in collector mock-up, *Magnetohydrodynamics* 3 (1989) 59-63.

[37] J. Reimann, L. Barleon, S. Molokov, I. Platnicks, E. Platacis, et al., First results from different investigations on MHD flow in multichannel U-bends, Proc. Seventh Beer-Sheva Intern. Seminar MHD Flows and Turbulence. Israel. 1993, to appear.

[38] S. Molokov, Liquid metal flows in manifolds and expansions of insulating rectangular ducts in the plane perpendicular to a strong magnetic field, KfK Report, KfK 5272 (1993).

[39] K. Miyazaki, K. Yokomizo, M. Nakano, T. Horiba, S. Inoue, et al., Heat transfer and pressure drop of lithium flow under longitudinal strong magnetic field, in: LIMET'88 (Avignon. 1988) pp. 436/1-11.

[40] V.G. Sviridov, Yu S. Shpansky and V.R. Tsoy, Liquid metal heat transfer under strong magnetic field, in: The 1992 Seminar on Liquid-Metal Magnetohydrodynamics (University of Tokyo, 1992) pp. 117-129.

[41] K. Miyazaki, H. Inoue, T. Kimoto, S. Yamashita, S. Inoue, et al., Heat transfer and temperature fluctuation of lithium flowing under transverse magnetic field, *J. Nucl. Sci. Technol.* 23 (1986) 582-593.

- [42] H. Branover and C. Henoch, Control of friction pressure losses and heat transfer in turbulent liquid metal flows in magnetic fields, in: Energy Transfer in Magnetohydrodynamic Flows. Proc. Conf. (Cadarache, France, 1991) pp.-389-394.
- [43] S. Malang, H.V. Borgstedt, E.H. Farnum, K. Natesan and I.V. Vitkovski. Development of insulating coatings for liquid metal blankets, in: Third International Symposium on Fusion Nuclear Technology (Los Angeles, 1994) p. 71.
- [44] I.A. Evtushenko, T.Q. Hua, I.R. Kirillov, C.B. Reed and S.S. Sidorenkov. The effect of magnetic field on heat transfer in a slotted channel, in: Third International Symposium on Fusion Nuclear Technology (Los Angeles, 1994) p. 72.
- [45] J. Reimann, L. Barleon, E. Bucenieks, L. Bühler, L. Lenhart, et al. MHD investigations related to a self-coded Pb-17Li blanket with poloidal-radial-toroidal ducts, in: Third International Symposium on Fusion Nuclear Technology (Los Angeles, 1994) p. 73.

Table 1. MHD Tests Conditions for Straight Channels

| No. | Channel cross-section | Dimensions ^[1] 2b×2a×l, mm ³ d×l, mm ² | Wall parameter, c | Magnetic field, T/ mean velocity, m/s | Liquid metal temperature, °C | Characteristic parameters ^[2] | Refer- ences |
|-----|-----------------------|---|----------------------|--|------------------------------------|--|-----------------|
| 1 | 2 | 3 | 4 | 5 | 6 | 7 | 8 |
| 1 | round | 21.2×500 | 0.083 | 1.5/≤1.3 | NaK, 20 | M≤840 Re≤1·10 ⁴ N≤80 | 12 |
| 2 | round | 45.3×500 | 0.04 | 0.3-1.75/2-15 | NaK, 20 | M≤2080 Re=(4-30)·10 ⁴ N≤110 | 13 |
| 3 | round | 28×500 | 0.06 | 0.3-1.75/2-15 | NaK, 20 | M≤1300 Re=(2.5-19)·10 ⁴ N≤70 | 13 |
| 4 | round | 15.75×500 | 0.069 | 0.1-1/0.5-5 | Li, 310-370 | M≤670 Re=(4.3-43)·10 ³ N≤105 | 14 |
| 5 | round | 130×1500 | 0.0364 0.0039 | 2/0.015-0.5 | NaK, 30 | M≤7600 Re=(0.6-20)·10 ³ N≤1·10 ⁵ | 15 |
| 6 | round | 108×1830 | 0.027 | 1-2/0.07-0.28 | NaK, 20 | M≤6400 Re=(4.1-16.5)·10 ³ N=620-1·10 ⁴ | 17 |
| 7 | round | 18×500 | 0 | 1.5/≤1.3 | NaK, 20 | M≤700 Re≤1·10 ⁴ N≤80 | 12 |
| 8 | rectangular | 20.5×45.5×500 | 0.0462 | 1.5/≤0.6 | NaK, 20 | M≤1800 Re≤1.25·10 ⁴ N≤260 | 18 |
| 9 | rectangular | 45.5×20.5×500 | 0.103 | 1.5/≤0.6 | NaK, 20 | M≤800 Re≤5700 N≤115 | 18 |

Table 1. Continued

| No. | Channel cross-section | Dimensions ^[1] 2b×2a×l, mm ³ d×l, mm ² | Wall parameter c | Magnetic field, T/ mean velocity, m/s | Liquid metal temperature, °C | Characteristic parameters ^[2] | Refer- ences |
|-----|----------------------------|---|--|--|------------------------------------|---|-----------------|
| 1 | 2 | 3 | 4 | 5 | 6 | 7 | 8 |
| 10 | rectangular | 15.7×15.7×500 | 0.0875 | 0.2-1.5/0.2-4 | Li, 309-380 | M≤1000 Re=(1.7-34)·10 ³ N≤600 | 19 |
| 11 | rectangular | 11.1×26.8×500 | 0.0517 | 0.2-1.5/0.2-4 | Li, 309-380 | M≤1700 Re=(2.9-58)·10 ³ N≤1000 | 19 |
| 12 | rectangular ^[3] | 10×100×600 | 0.046 0.019 0 | 0.4-1.0/0.02-0.45 | InGaSn | M≤1520 Re=(1.7-47)·10 ³ N≤840 | 20 |
| 13 | rectangular | 87.8×87.8×1830 | 0.07 | 1.1-2.3/0.006-0.34 | NaK, 20 | M≤5.8·10 ³ Re=(0.23-16)·10 ³ N≤1.26·10 ⁵ | 17, 21 |
| 14 | rectangular ^[3] | 14×140×1830 | c ₁ =6.7·10 ⁻³ c ₂ =4·10 ⁻² | 1-2/0.05-0.7 | NaK, 20 | M≤8.2·10 ³ Re=(0.7-53)·10 ³ N≤1·10 ⁵ | 22 |
| 15 | rectangular | 19.5×43.5×700 | 0 (three electrically insulated walls) | 1.5/≤0.6 | NaK, 20 | M≤1700 Re≤1.2·10 ⁴ N≤240 | 18 |
| 16 | rectangular | 3.0x×100x×600 | 0 | 0.3-1.1/0.02-2.3 | InGaSn | M≤1740 Re=(0.2-24)·10 ⁴ N≤1200 | 20 |
| 17 | rectangular | 100×60×1830 | c=C ₂ =2.3×10 ⁻² C ₁ =2.75 | 0.5-2/0.038-0.44 | NaK, 20 | 900<M<3400 93<N<9300 | * |

Notes: ^[1] length of magnetic field; ^[2] characteristic length — a or d/2; ^[3] the same channels were also tested with anchor links;
* previously unpublished results from KfK/ANL Flow Tailoring Test Section [30,31] constant area section downstream of variable area section

Table 2. Comparison of Measured and Calculated Values of k_p for Channels of Table 1

| Channel No. | 1 | 2 | 3 | 4 | 5a ^[1] | 5b | 6 | 8 | 9 | 10 | 11 | 12 ^[2] | 13 | 17 |
|---------------------------|------|------|------|------|-------------------|------|------|------|-------|------|------|-------------------|------|------|
| $k_{p.exp} \cdot 10^3$ | 80.7 | 40 | 56.1 | 64.5 | 37.8 | 4.72 | 24.6 | 26.5 | 72.0 | 61.6 | 28.7 | 3.97 | 52.4 | 22.3 |
| $k_{p.theory} \cdot 10^3$ | 76.6 | 38.5 | 56.6 | 64.5 | 35.1 | 3.88 | 25.3 | 25.9 | 81.9 | 61.6 | 27.8 | 4.37 | 51.9 | 21 |
| $\Delta k_p, \%$ | 6.3 | 3.8 | -0.9 | 0 | 7.1 | 17.8 | -2.8 | 2.3 | -13.8 | 0 | 3.1 | -10 | 0.95 | 6 |

Notes: ^[1] $c=0.0364$ (5a), $c=0.0039$ (5b); ^[2] $c=0.019$

Table 3. MHD Tests Conditions for Channels of Complex Geometry

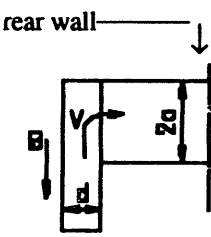
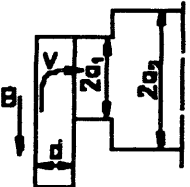
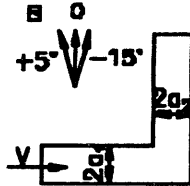
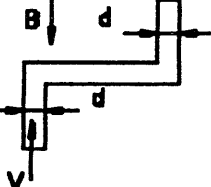
| No. | Geometry | Dimensions, mm | Wall parameter, c | Magnetic field, T/ mean velocity, m/s | Liquid metal temperature, °C | Characteristic parameters | References |
|-----|--|---|----------------------|--|------------------------------|--|------------|
| 1 | right angle bend  | $2b \times 2a = 7 \times 70$ $d = 20$ $L = 2b$ | 0.120 | $\leq 4 / 0.2 - 1.2$ | GaInSn, 25 | $M \leq 10^3$ $Re = (0.4 - 2.5) \cdot 10^4$ $N \leq 200$ | 32 |
| 2 | right angle bend and sharp change of cross section  | $2b \times 2a_1 (2a_2) = 7 \times 70 (350)$ $d = 19.2$ $L = 2b$ | 0.12 | $\leq 4 / \leq 0.5$ | GaInSn, 25 | $M \leq 10^3$ $Re \leq 10^4$ $N \leq 1485$ | 32 |
| 3 | right angle bend  | $2b \times 2a_1 (2a_2) = 76.2 \times 76.2 (50.8)$ $L = 2b$ | 0.055 | $\leq 3.5 / \leq 0.76$ | NaK, 30 | $M \leq 1.6 \cdot 10^4$ $Re = (1.2 - 60) \cdot 10^3$ $N \leq 1.2 \cdot 10^5$ | 33 |
| 4 | z-type bend  | $L = d = 60$ | $1.67 \cdot 10^{-2}$ | $\leq 2 / \leq 1$ | Na, 250 | $M \leq 1.5 \cdot 10^4$ $Re \leq 1.7 \cdot 10^5$ $N \leq 5 \cdot 10^4$ | 34 |

Table 3. Continued

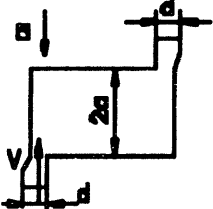
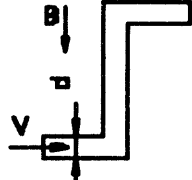
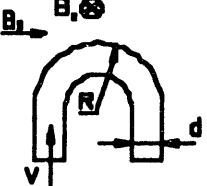
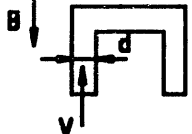
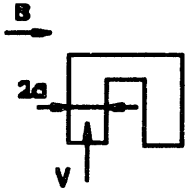
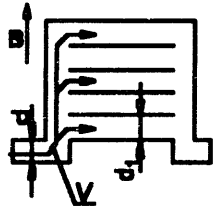
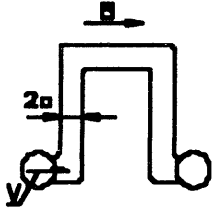
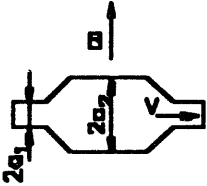
| No. | Geometry | Dimensions, mm | Wall parameter, c | Magnetic field, T/ mean velocity, m/s | Liquid metal temperature, °C | Characteristic parameters | References |
|-----|--|------------------------|-----------------------|--|------------------------------|--|------------|
| 5 | z-type bend  | 2b×2a=25×100 L=d=60 | 1·10 ⁻² | ≤2/≤1 | Na, 250 | M≤1.5·10 ⁴ Re≤1.7·10 ⁵ N≤9·10 ⁴ | 34 |
| 6 | z-type bend  | L=d=21 | 0 | -/≤0.15 | GaInSn, 25 | M≤1600 Re=(0.65-9)·10 ³ N≤5·10 ³ | 35 |
| 7 | U-turn  | L=d=21 R/d=1.85 | 0 | ≤1.5/≤3 | Hg, 20 | M≤720 Re=10 ³ -6·10 ⁵ N≤180 | 8 |
| 8 | U-turn  | L=d=60 | 1.67·10 ⁻² | ≤2/≤1 | Na, 250 | M≤1·10 ⁴ Re≤1.7·10 ⁵ N≤2.5·10 ⁴ | 34 |

Table 3. Continued

| No. | Geometry | Dimensions, mm | Wall parameter, c | Magnetic field, T/ mean velocity, m/s | Liquid metal temperature, °C | Characteristic parameters | References |
|-----|--|--|-------------------------------|--|------------------------------|--|------------|
| 9 | U-turn  | $2b \times 2a = 120 \times 11.5$ $L = 2b$ | 0 | $\leq 1.7 / \leq 0.3$ | Hg, 20 | $M \leq 4680$ $Re = 500 - 3 \cdot 10^5$ $N \leq 4 \cdot 10^4$ | 8 |
| 10 | U-turn manifold  | $L = d = 26$ $d_1 = 10$ | -0 | $\leq 2 / \leq 2.8$ | GaInSn, 25 | $M \leq 650$ $Re = (2.5 - 100) \cdot 10^3$ $N \leq 70$ | 36 |
| 11 | U-turn manifold  | $2b \times 2a = 25 \times 25$ $L = 2b$ number of parallel channels $n = 1; 2; 3; 5$ | 0.038 | $\leq 3.6 / \leq 0.37$ | NaK, 30 | $M \leq 4000$ $Re = (1 - 9.6) \cdot 10^3$ $N \leq 4 \cdot 10^4$ | 37 |
| 12 | Expansion contraction  | $2b \times 2a_1 (2a_2) =$ $100 \times 60 (140)$ $L = 2b$ | $c_1 = 0.014$ $c_2 = 1.65$ | $\leq 2 / 0.24$ | NaK, 20 | $M \leq 1.2 \cdot 10^4$ $Re = 720 - 2.2 \cdot 10^4$ $N = 400 - 2 \cdot 10^5$ | 30, 31 |

07

Table 4. HT Test Conditions

| No. | Channel cross-section | Dimensions ^[1] d ₁ ×d ₂ ×l, mm ² 2b×2a×l, mm ³ | Magnetic field, T | Liquid metal temperature, °C | Mean velocity, m/s | Heat flux, w/cm ² | Characteristic parameters ^[2] | References |
|-----|-----------------------|---|-------------------|------------------------------|--------------------|------------------------------|---|------------|
| 1 | ring | 15.8/7.6×300 | axial, ≤5 | Li, 350-450 | ≤4 | ≤70 | M≤3.6·10 ³ Re≤4·10 ⁴ N≤5·10 ³ Pr=3.4·10 ⁻² | 39 |
| 2 | round | 19×1330 | axial, ≤1 | Hg, 30 | ≤0.25 | ≤3.5 | M≤500 Re≤2·10 ⁴ N≤30 Pr=2.3·10 ⁻² Ra≤2·10 ⁴ | 40 |
| 3 | ring | 15.8/7.6×300 | transverse, ≤1 | Li, 320-390 | ≤4 | ≤68 | M≤700 Re≤5·10 ⁴ N≤245 Pr=3.6·10 ⁻² | 41 |
| 4 | rectangular | 14×140×914 | transverse, ≤2 | NaK, 20-80 | ≤0.7 | ≤9.5 | M≤820 Re≤5.3·10 ³ N≤1·10 ⁴ Pr=2.4·10 ⁻² | 22 |

Note: ^[1] heater length; ^[2] characteristic length L=d₁-d₂ for Nos. 1 and 3, L=d for No. 2, L=b for No. 4.

17

Figure Captions

- Fig. 1 Rectangular duct geometry.
- Fig. 2 Velocity profiles (theory and experiment) for channels of Table 1:
1-channel No. 12, 2-channel No. 14
- Fig. 3 Insulating wall channel characteristics in inclined transverse magnetic field at $M=1100$:
1 and •••- theory and experiment for $\lambda^* = f(\theta)$,
2 and xxx- theory and experiment for $\zeta_1 = f(\theta)$
- Fig. 4 Theory and experiment for round duct transverse velocity profile in the fringing magnetic field ($x-U/U_0$ in uniform magnetic field region).
- Fig. 5 Theory and experiment for axial pressure gradients in round (1 and •••) and rectangular (2 and +++) ducts.
- Fig. 6 Experimental data for pressure drag coefficient in rectangular duct with insulating walls in fringing magnetic field.
- Fig. 7 Boundary curve for transition from inertial to non-inertial flow in insulating wall rectangular duct in fringing magnetic field.
- Fig. 8 Transverse velocity profile for rectangular duct flow tailoring:
1 and xxx - in the middle of expansion,
2 and --- in the constant cross-section duct part.

- Fig. 9 Boundary curves for transition from inertial to non-inertial flow in ducts of complex geometry.
- Fig. 10 Asymptotic values of ζ/N in ducts of complex geometry (nomenclature is the same as for Fig. 9).
- Fig. 11 Heat transfer intensification with thermogravitational convection in a round duct.
- Fig. 12 Temperature fluctuations in a round duct.
- Fig. 13 Experimental data for \bar{Nu} (\times, \square) and temperature fluctuations ($^{\circ}, \bullet$) in a round duct.
- Fig. 14 Temperature profiles at $y=0$ and $z/L=-1.86$ (theory and experiment) for rectangular heated duct.

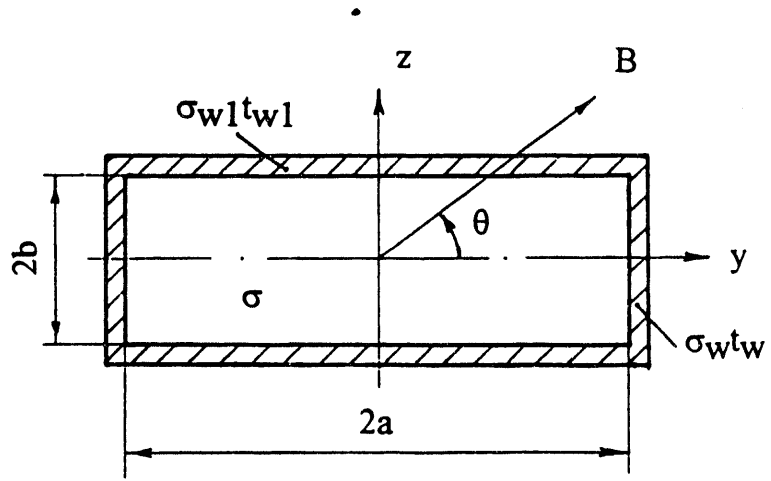


Fig.1 I.R.Kirillov et al. "Present understanding..."

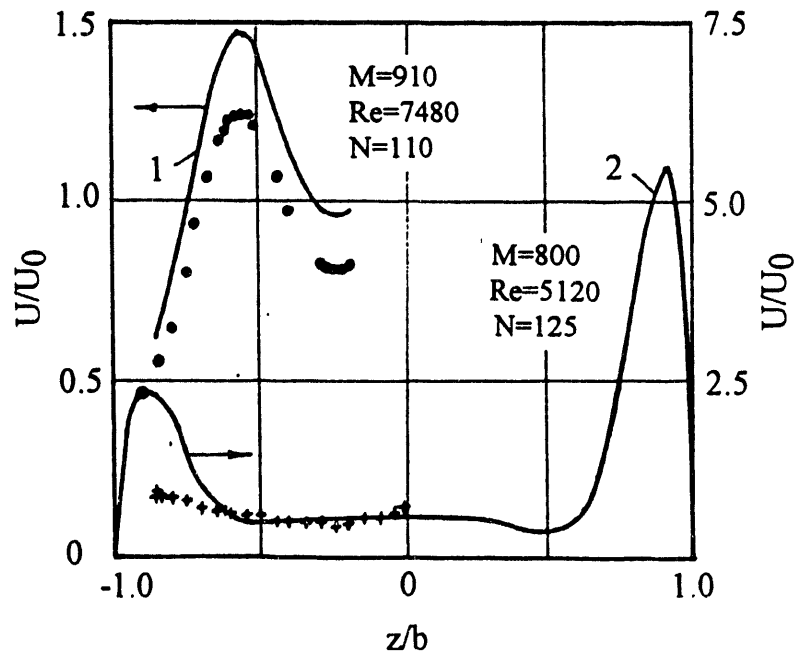


Fig.2 I.R.Kirillov et al. "Present understanding..."

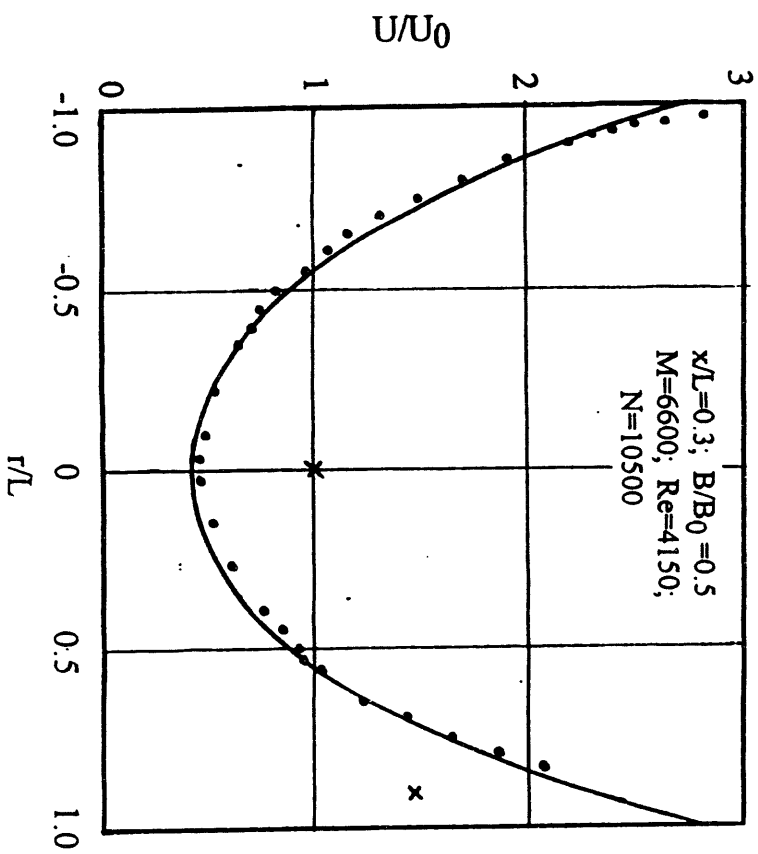


Fig.4 I.R.Kirillov et al."Present understanding..."

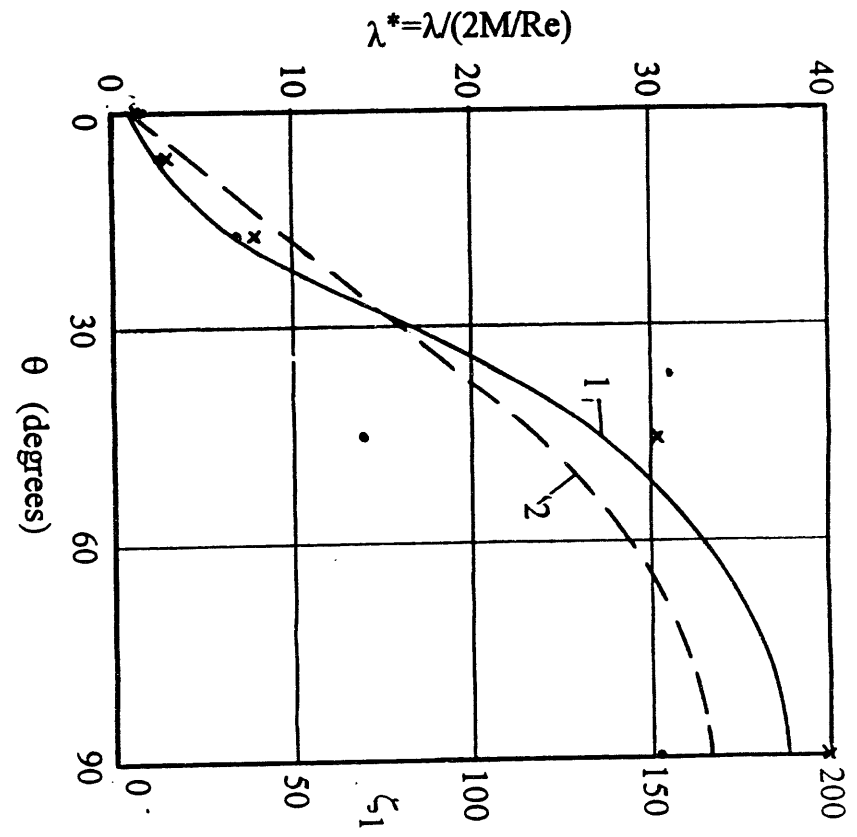


Fig.3 I.R.Kirillov et al."Present understanding..."

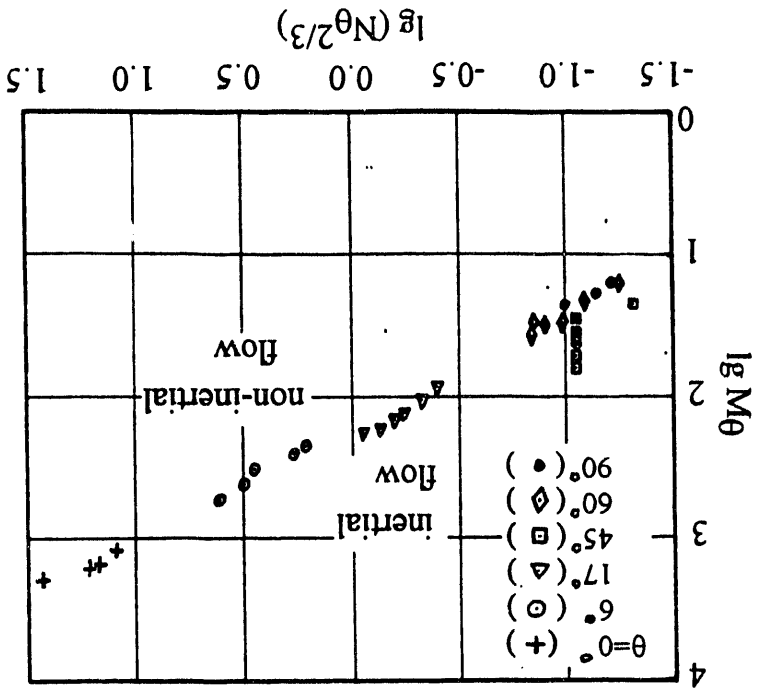


Fig. 7 I.R. Kirillov et al. "Present understanding..."

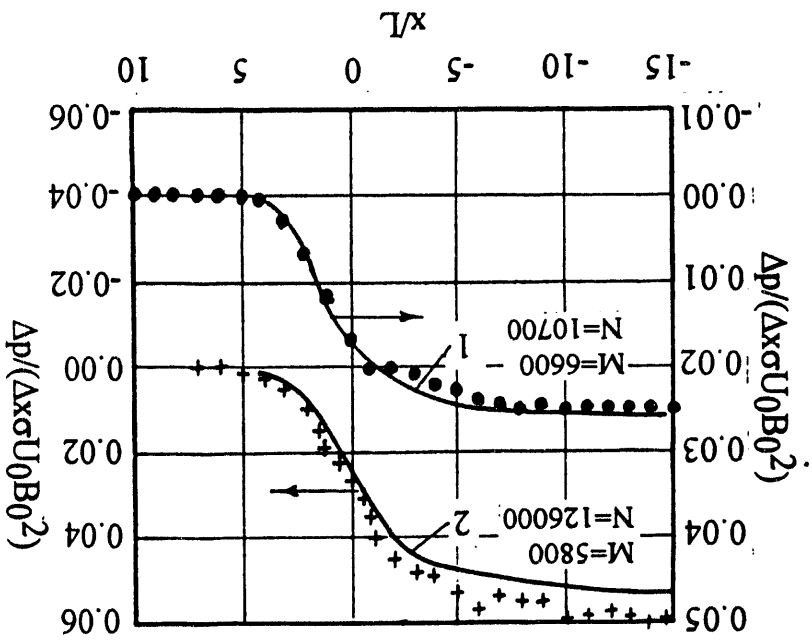


Fig. 5 I.R. Kirillov et al. "Present understanding..."

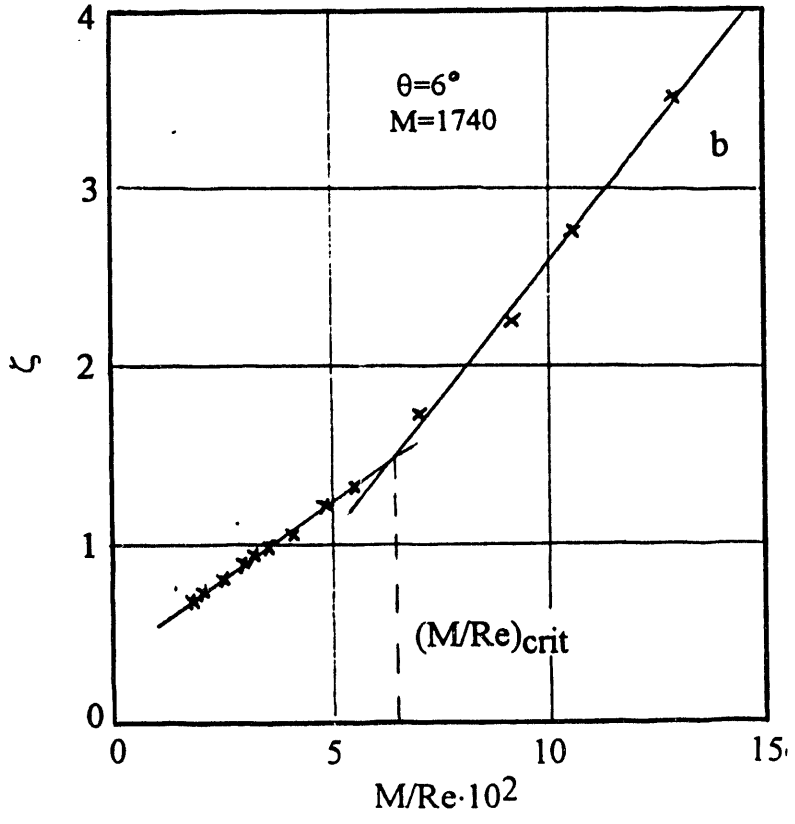
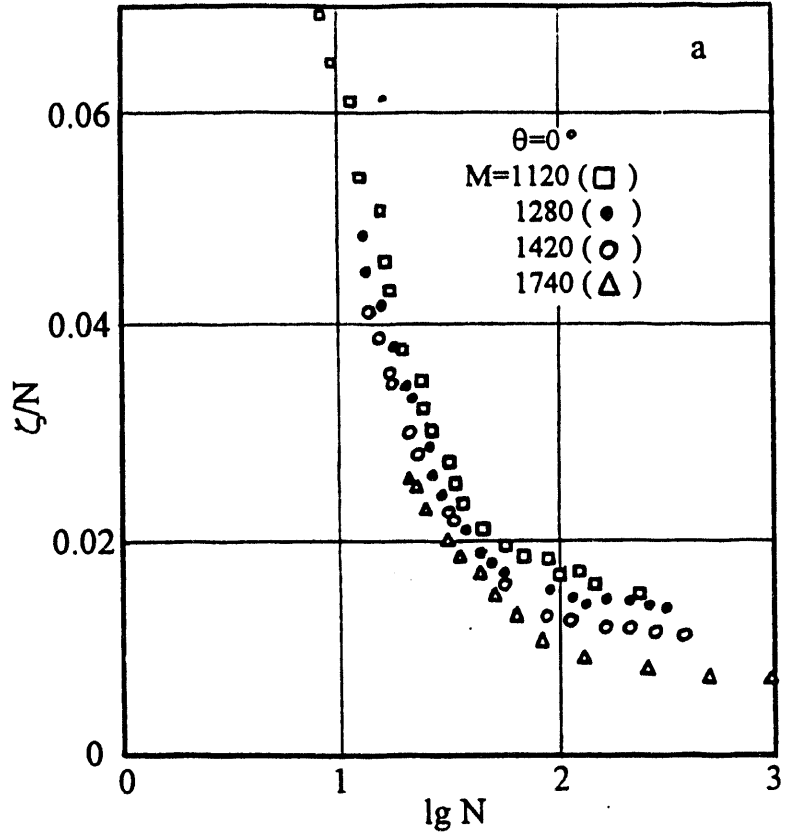


Fig.6 I.R.Kirillov et al. "Present understanding..."

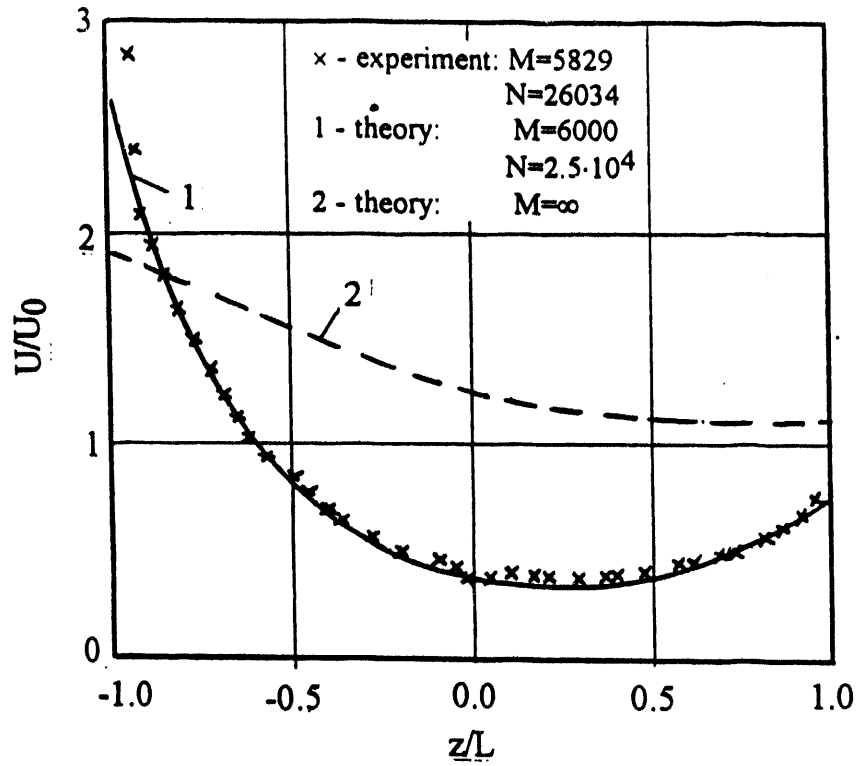


Fig. 8 I.R. Kirillov et al. "Present understanding..."

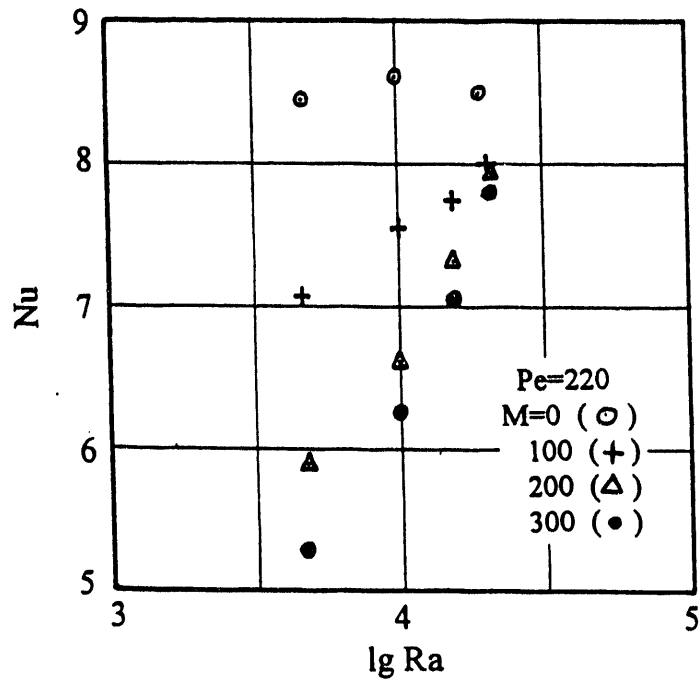


Fig. 9 I.R. Kirillov et al. "Present understanding..."

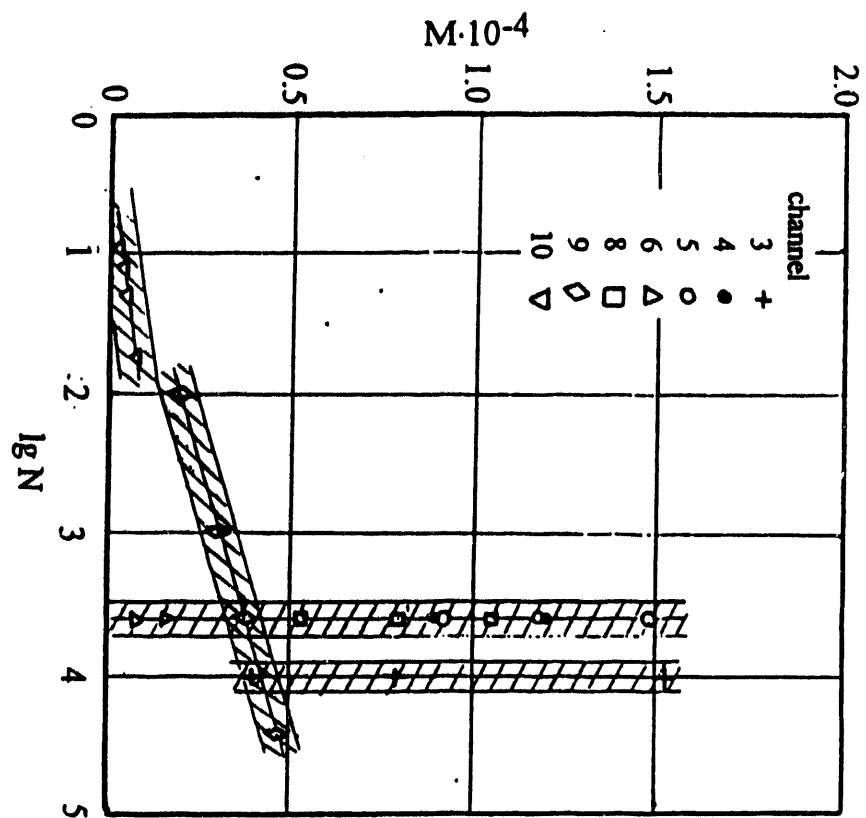


Fig.9 I.R.Kirillov et al."Present understanding..."

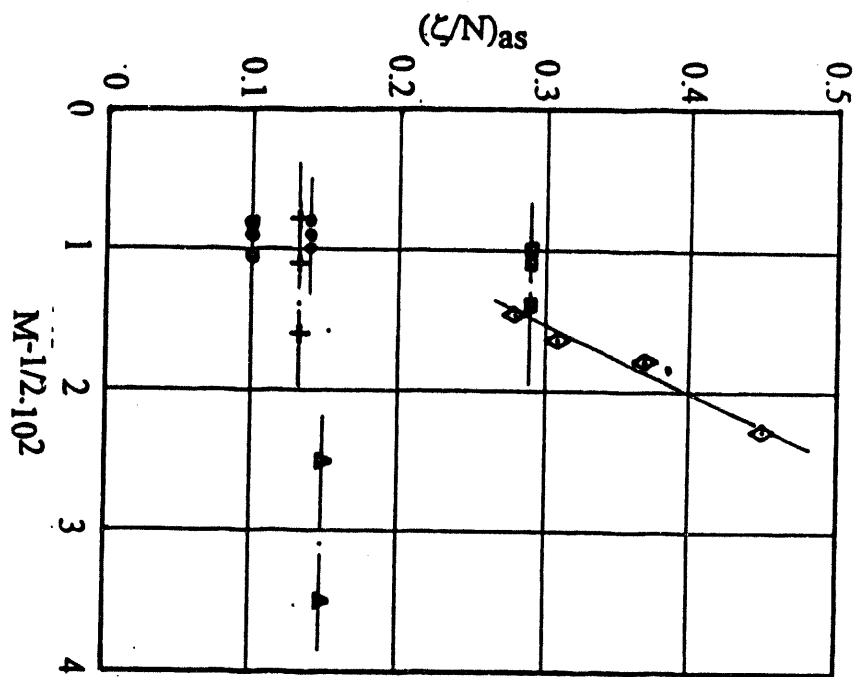
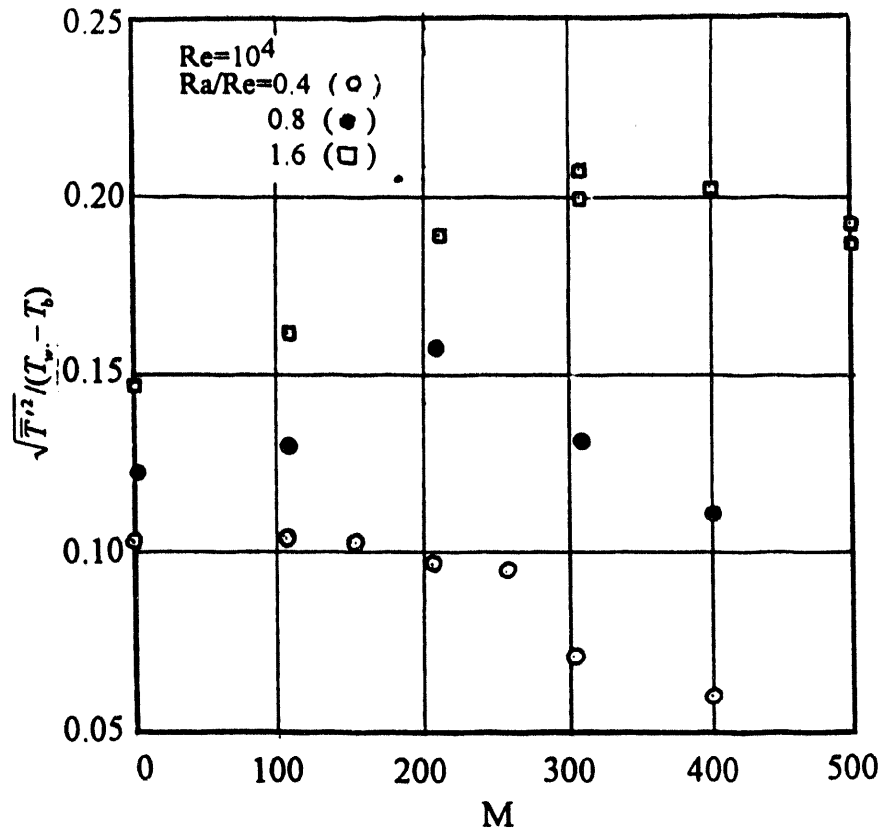
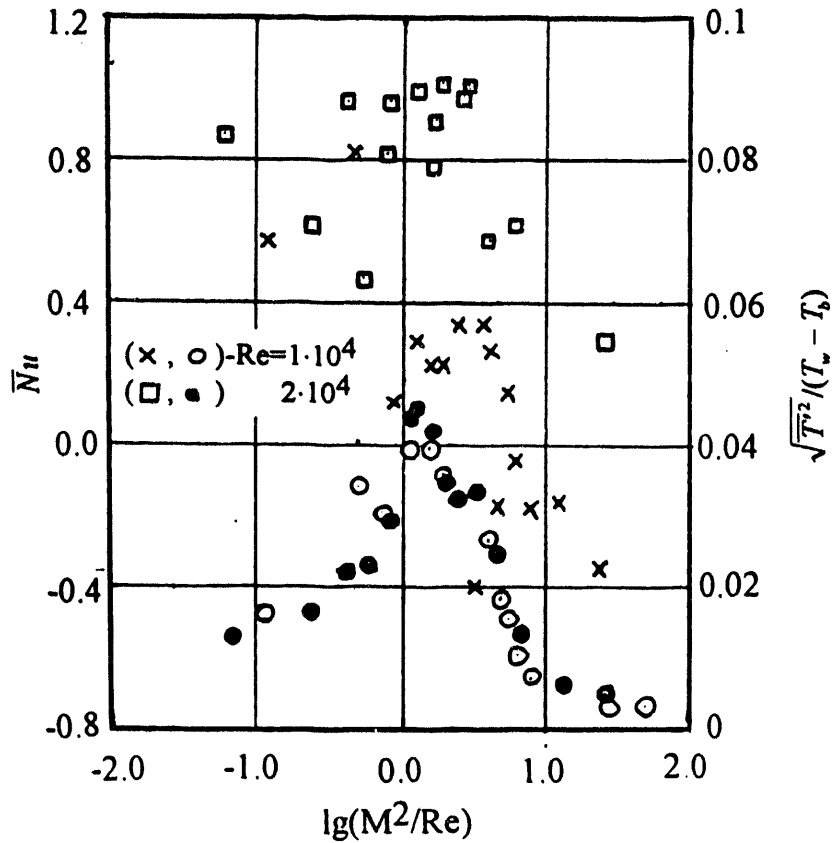


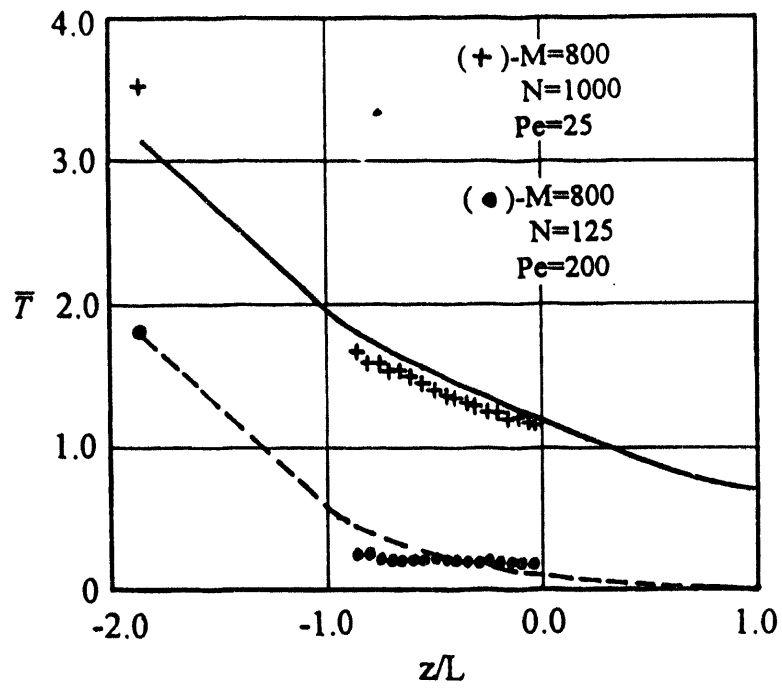
Fig.10 I.R.Kirillov et al."Present understanding..."



12
 Fig. I.R. Kirillov et al. "Present understanding..."



13
 Fig. I.R. Kirillov et al. "Present understanding..."



14
 Fig. 14 I.R. Kirillov et al. "Present understanding.."

DATE

FILMED

10/18/94

END

